Nonlinear model predictive control (NMPC) of the solvent-based post-combustion CO_2 capture process

Toluleke E Akinola[a], Eni Oko[a,b], Xiao Wu[a,c], Keming Ma[a,d], Meihong Wang[a,*]
[a] Department of Chemical and Biological Engineering, University of Sheffield, Sheffield. S1 3JD
[b] Department of Chemical Engineering, University of Hull. HU6 7RX
[c] Key laboratory of Energy Thermal Conversion and Control of Ministry of Education, Southeast University, Nanjing 210096, China
[d] Wood Plc, Shinfield Park, Reading, UK. RG2 9FW
* Corresponding Author. Tel.: +44 114 222 7160. E-mail address: Meihong.Wang@sheffield.ac.uk

Abstract

The flexible operation capability of solvent-based post-combustion capture (PCC) process is vital to efficiently meet the load variation requirement in the integrated upstream power plant. This can be achieved through the deployment of an appropriate control strategy. In this paper, a nonlinear model predictive control (NMPC) system was developed and analysed for the solvent-based PCC process. The PCC process was represented as a nonlinear autoregressive with exogenous (NARX) inputs model, which was identified through the forward regression with orthogonal least squares (FROLS) algorithm. The FROLS algorithm allows the selection of an accurate model structure that best describes the dynamics of the process. The simulation results showed that the NMPC gave better performance compared with linear MPC (LMPC) with an improvement of 55.3% and 17.86% for CO_2 capture level control under the scenarios considered. NMPC also gave a superior performance for reboiler temperature control with the lowest ISE values. The results from this work will support the development and implementation of NMPC strategy on the PCC process with reduced computational time and burden.

Keywords: Post-combustion carbon capture; chemical absorption; nonlinear system identification; Nonlinear MPC; FROLS-ERR; Flexible operation

Highlights

- Nonlinear system identification carried out using NARX model
- FROLS-ERR algorithm implemented to select significant model terms
- NMPC developed for solvent-based CO_2 capture process
- Performance evaluation of NMPC under flexible operation scenario

Nomenclature

$e(t)$	Noise sequence
$f(\cdot)$	Nonlinear function
N	Number of samples in a training data set
n_{CO_2}	Mass fraction of CO_2 in the flue gas
n_e	Maximum lag for the system noise
n_u	Maximum lag for the system input
n_y	Maximum lag for the system output
r	Number of input variables
$u(t)$	System input
$x_{rj}(t)$	Regressor vector
$y_r(t)$	Response signal (output)

Greek letter

φ_{rj}	Model parameter

Superscript

ABS_{in}	Absorber inlet
ABS_{out}	Absorber outlet

Abbreviations

BIC	Bayesian information criterion
CL	capture level
CV	Controlled variable
ERR	Error reduction ratio
FROLS	Forward regression orthogonal least square
LMPC	Linear model predictive control
MEA	Monoethanolamine

MIMO	Multiple-input-multiple-output
MPC	Model predictive control
MPO	Model prediction output
NARX	Non-linear auto-regressive with exogenous input
NMPC	Nonlinear model predictive control
PCC	Post-combustion carbon capture
PI	Proportional Integral
PID	Proportional Integral Derivative
SI	System identification

1. Introduction

1.1 Background

Fossil fuel combustion for electricity and heat generation is the biggest culprit for anthropogenic CO_2 emissions, which is regarded as a major contributor to global warming [1]. Atmospheric CO_2 could reach catastrophic levels in the future if CO_2 emission continues unabated[2]. Carbon capture, CO_2 utilisation and storage (CCUS) is considered the most strategic technology for sustainably and economically meeting carbon emission reduction targets [3]. Among various CCUS technologies, solvent-based post-combustion CO_2 capture (PCC) has gained much attention as the suitable technology to treat flue gas from fossil fuel-fired power plant. This is attributed to its maturity and its suitability to be retrofitted to existing fossil fuel power plants. Monoethanolamine (MEA) has generally been considered as a benchmark solvent for solvent-based PCC technology. However, the energy required for solvent regeneration is a major challenge as it contributes to a significant drop in power plant efficiency [4]. This can be addressed through the implementation of an appropriate control strategy in the solvent-based PCC process. The solvent-based PCC process is inherently nonlinear and thus requires the implementation of a nonlinear model predictive control (NMPC).

1.2 Literature review

Existing studies on solvent-based PCC process control have focused mostly on the PI/PID control implementation in the process [5–11]. This is due to the simplicity of PI/PID controllers and the vast experience with their implementation in the process industry. However, PI/PID control are implemented via isolated control loops and does not adequately account for loop

interactions[12]. This limits the operating capability of these controller designs in achieving stable conditions within short intervals of load change. The PI/PID control parameters are generally set based on a given load condition and its control performance also degrades quickly due to the frequent changes in load or other operating parameters. To deal with these issues, model-based predictive (MPC) is considered a better approach for solvent-based PCC process.

MPC scheme mainly makes use of the explicit process model to determine process output, based on the calculation of control sequence, by minimizing an objective function [13]. This indicates that the accuracy of the process model is key to achieving a suitable MPC controller performance. The MPC can be categorized into Linear MPC (LMPC) and nonlinear MPC (NMPC) [14]. The LMPC scheme utilizes a linear model to predict the PCC process dynamics, while NMPC utilizes a nonlinear model [15]. Performance evaluation comparison of LMPC with decentralised PI/PID control showed that the LMPC scheme gave a better and faster performance [9,10,14,16–20]. This has given rise to extensive implementation of LMPC on the solvent-based PCC process[12,16,18–22]. However, the linear model is unable to predict the nonlinear behaviour of the nonlinear PCC plant, especially during flexible operation, where the operating point deviates from the design-operating region by a large magnitude. This results in a modelling mismatch and eventually causes deterioration of the solvent-based PCC control performance, which has motivated the need for NMPC.

NMPC has enormous potential for application in the solvent-based PCC process, which has been identified to exhibit strong nonlinearities and is required to frequently change at several operation regimes in accordance with market demands. This is due to the capacity of NMPC to deal with nonlinear dynamics by representing the solvent-based PCC as a nonlinear model. A few studies on NMPC for solvent-based PCC utilized a first principle model as the prediction model [21–24]. In these publications, the first-principles models were simplified for efficient online NMPC optimization. Control performance evaluation carried out displayed the feasibility of the NMPC implementation for solvent-based PCC process. However, the high computational burden and time necessary for the first principles model development as well as the online implementation of the NMPC algorithm is technically challenging. To address this Challenge, a few studies adopted a data-driven model developed via system identification as the prediction model for NMPC implementation [4,14].

Wu et al.[14] presented a multi-model predictive control (MMPC) strategy to deal with the nonlinearity within the solvent-PCC process at a wide flexible operational range. The MMPC strategy was designed based on the nonlinearity analysis, which gives the nonlinearity distribution for a wide range of operation. The MMPC strategy includes 3 local state-space models combined and scheduled through a fuzzy membership function calculated by the CO_2

capture level. Simulation results showed that the MMPC strategy gave a better performance than the Linear MPC. However, modelling mismatch was inevitable, although MMPC was able to reduce offset better than the linear MPC.

Zhang et al.[4] implemented NMPC scheme on a nonlinear additive autoregressive with exogenous input (NAARX model). The NMPC strategy gave a superior performance in comparison with Linear MPC by a small margin. The limitation in the improvement was due to the challenge of obtaining a satisfactory NAARX with suitable cross-terms that accurately capture the nonlinear dynamics of the solvent-based PCC process [12].

To tackle the issues highlighted above, this paper adopted the Forward Regression Orthogonal Least Square – Error Reduction Ratio (FROLS-ERR) algorithm approach for developing a transparent parsimonious NARX model that captures the relationship between the input and output variables in the CO_2 capture process. The FROLS-ERR algorithm selects the important model terms, in a stepwise manner, based on their significance, measured based on ERR [25]. Hence, insignificant model terms are eliminated thus reducing the complexity of the model.

1.3 Aim and Novel Contribution

In this study, NMPC was implemented on the solvent-based PCC process to evaluate its performance in comparison with LMPC. The NMPC utilized a nonlinear model developed using FROLS-ERR algorithm. The novel contributions of the paper are listed as follows:

1. Parsimonious model development for solvent-based PCC process using FROLS-ERR algorithms, which selects the significant model terms that best describe the system dynamics.
2. Couplings between the controlled (output) variables were accounted for in the model. This is to improve the prediction accuracy of the model.
3. NMPC is designed for a wide range of operation based on the parsimonious model developed via FROLS-ERR
4. The control performance of the NMPC is demonstrated to be better than LMPC through the case study.

2. Data-driven model development of the solvent-based PCC process

2.1 Solvent-based PCC model Description

The first principle model of the solvent-based PCC process using MEA developed by Lawal et al.[1] was used for the control system design and implementation. The model was dynamically validated by Biliyok et al.[26]. Fig 1 shows a schematic diagram of the solvent-based PCC

process. Insights gained from previous studies on the CO_2 capture process was vital in identifying key process variables that are sensitive to the dynamic performance of the capture plant for flexible operation mode [1].

For the MPC control system design, the control objective functions of the solvent-based PCC process are usually centred on environmental and economic targets. The key output variables sensitive to the control objectives are the CO_2 capture level and reboiler temperature. The CO_2 capture level (CO_2-CL) measures the amount of CO_2 captured from the capture plant and can be expressed mathematically as follows:

$$CO_2\text{-CL}= \left(1 - \frac{n_{CO_2}^{ABS_{out}} \times F_{CO_2}^{ABS_{out}}}{n_{CO_2}^{ABS_{in}} \times F_{CO_2}^{ABS_{in}}}\right) \times 100\% \quad (1)$$

The reboiler temperature is closely related to the lean solvent loading, which determines the CO_2 absorption capacity in the absorber [14]. Also, controlling the reboiler temperature is relevant to limiting solvent degradation in the reboiler [27]. Lean solvent flowrate and steam flowrate were selected as the manipulated variables based on their strong influence on the CO_2 capture level and reboiler temperature respectively[1,28].

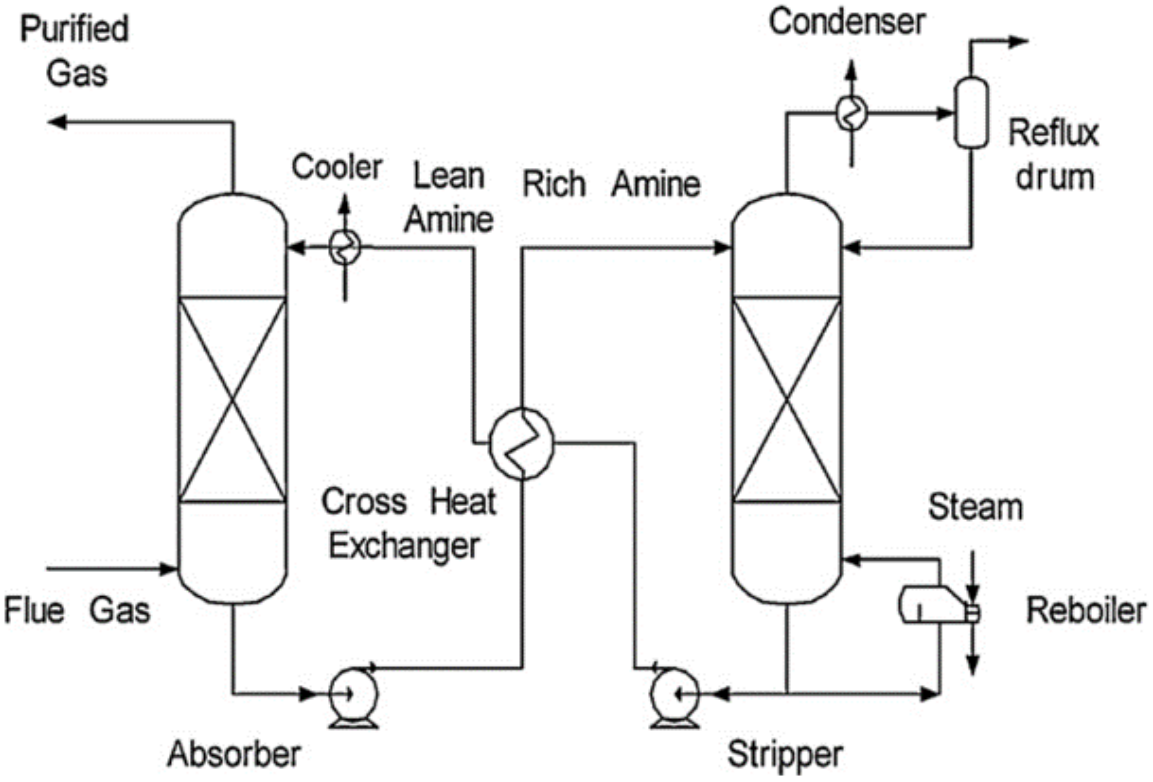

Fig 1 Solvent-based PCC process[1]

2.2 Data-driven model development of the solvent-based PCC process using FROLS-ERR

The multivariable NARX input model, which is a special form of Nonlinear auto-regressive moving with exogenous input (NARMAX) model, is adopted to represent the solvent-based PCC process. This is due to its suitability to represent a large range of nonlinear systems [29]. The MIMO-NARX model is described as[29]:

$$y_i(t) = f_i\,(y_i(t-1),\dots,y_1(t-n_y),\dots,y_s(t-1),\dots,y_s(t-n_y),u_1(t),u_1(t-1),\dots,u_1(t-n_u),\dots,u_r(t),u_r(t-1),\dots,u_r(t-n_u)) \;+\; e_i(t) \tag{2}$$

where r is the number of external input signals and s is the number of output signals; $y_i(t)$,$u_j(t)$ and $e(t)$, with $i = 1,2,..s$, $j = 1,2,\dots,r$ and $t = 1,2,\dots,N$ are measured system outputs, inputs and unmeasurable noise sequences, respectively; n_y and n_u are the maximum lags in the output and input; $f(\cdot)$ represents a nonlinear function, which is generally unknown but can be approximated using various types of nonlinear forms. Polynomial expansion of $f(\cdot)$ is most commonly used due to its good properties including transparency and easy interpretation of the model [30]. The solvent-based PCC process considered in the present study is a typical MIMO system, involving three inputs (flue gas flowrate, lean solvent flowrate and steam flowrate) and two outputs (CO_2-CL and T_{reb}) as shown in Fig 2. The MIMO-NARX model is described in Eq (2) such that the loop interaction between the output variables are accounted for. For each output variable, the NARX model can be re-arranged into a linear-in-the-parameters form as:

$$y_s(t) = \sum_{j=1}^{M_r} \varphi_{rj} x_{rj}(t) + \; e_r(t) \tag{3}$$

where $y_s(t)$, $x_{rj}(t)$, φ_{rj} and M_r, with $(s = 1,2;\ r = 1,2,3; j = 1,2,\dots,M_r)$, are the response signals (outputs), regressors, model parameters and number of model terms. Each φ_{rj} is built using lagged input and lagged output variables, such as $y_2(t-1), y_1(t-1)^2, y_1(t-1)y_2(t-3), u_1(t-1)u_2(t-1), y_2(t-1)u_3(t-1)$, etc. FROLS was adopted to select significant model terms for the MIMO system based on ERR. Details on FROLS algorithm procedure for model structure selection can be seen in [25,30,31].

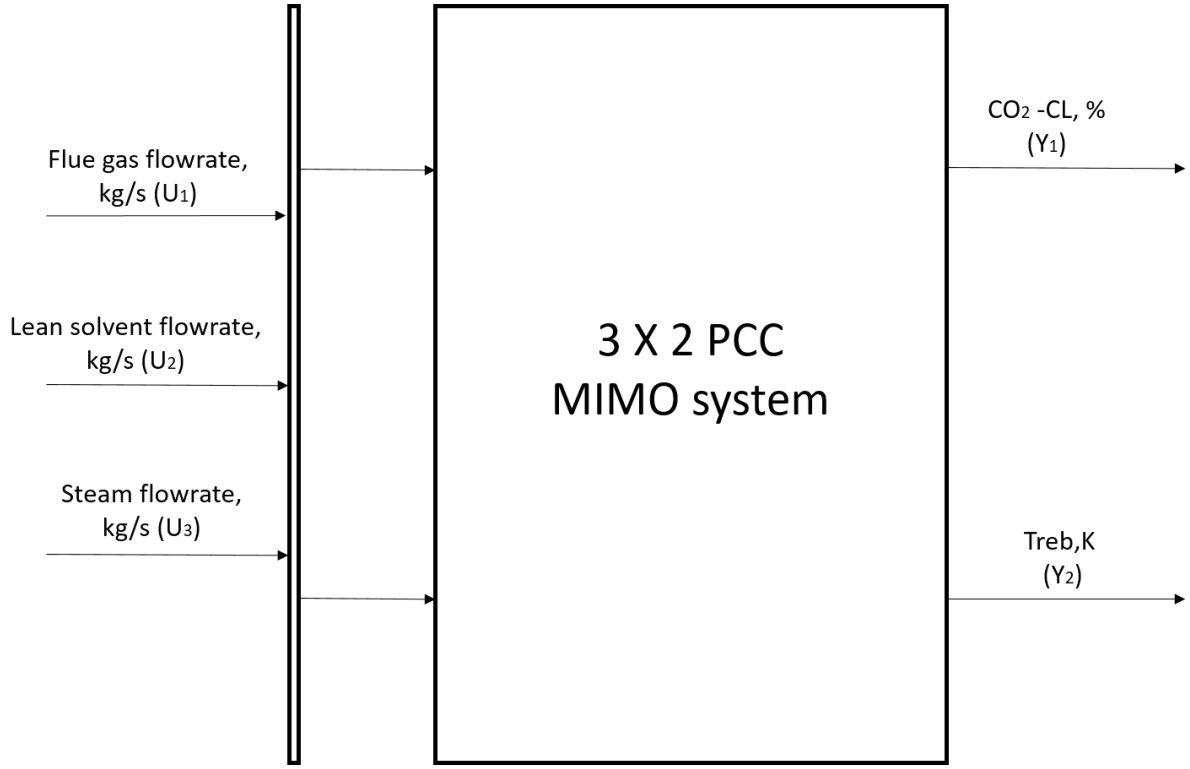

Fig 2 MEA-based PCC model represented as a Multiple-Input Multiple-output (MIMO) system; U_1-Flue gas flowrate (kg/s); U_2- Lean solvent flowrate (kg/s); U_3- Stream flowrate (kg/s); Y_1- CO_2-CL (%); Y_2-Treb (K).

Uniformly distributed random noise signals were designed for the input variables and implemented on the gPROMS® model developed by Lawal et al.[1]. These signals span the amplitude range of the input variables uniformly, which is important for the identification of a nonlinear system. Data generated at a sampling interval of 60s were collected for nonlinear system identification. The sampling interval was selected such that the sample rate is greater than twice the maximum frequency of interest within the system (which is equivalent to the low dominant time constant).

For each NARX model term development, the maximum time lags for the input and output variables for both subsystem 1 and 2 were selected to be $n_y = n_u = 3$ and $n_y = n_u = 2$ respectively. The degree of nonlinearity was selected to be 2. The values of $n_y \; and \; n_u$ for both sub-systems are large enough to cover the range of potential time lags needed to represent the CO_2 capture process dynamics. Model terms were ranked based on their level of significance (using ERR index) to the output variables. BIC is used to determine the number of model terms[25,32]. BIC implements a more rigorous penalty on each model term to avoid over-fitting compared to other model selection criteria. The FROLS-ERR stops at minimum BIC.

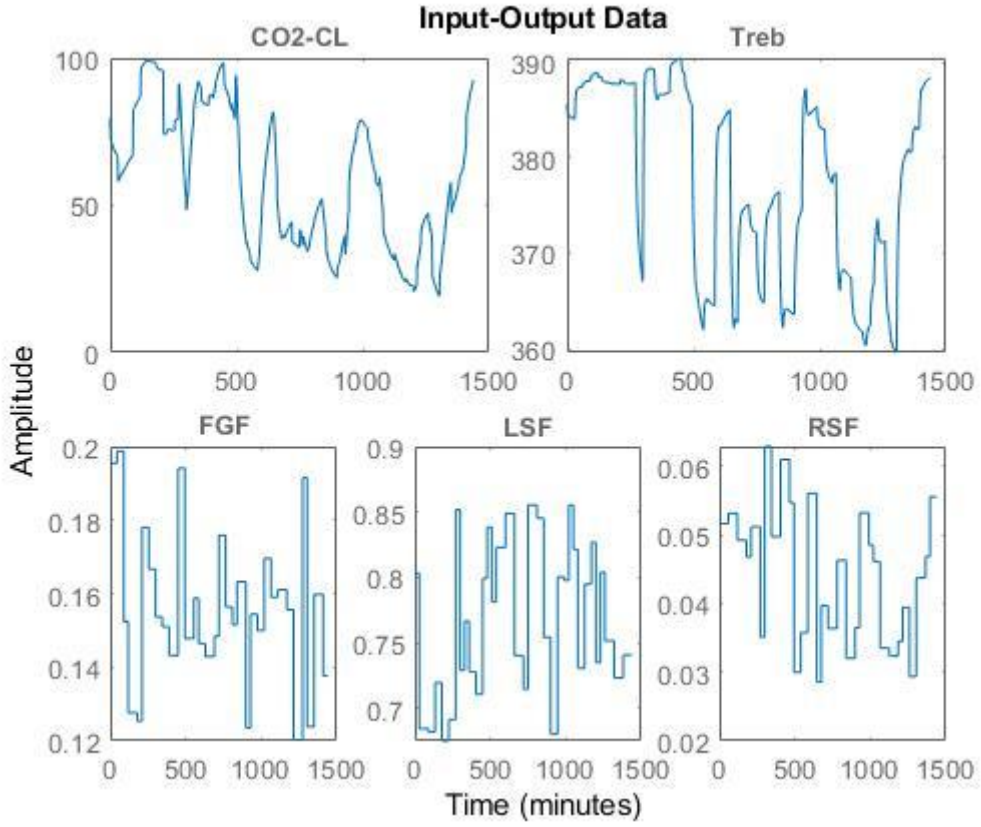

Fig 3 Input-output data obtained from an MEA-based PCC model developed in gPROMs; CO_2-CL, %: CO_2 Capture level; T_{reb}: reboiler temperature, K; FGF: flue gas flowrate, kg/s; LSF: lean solvent flowrate, kg/s; RSF: reboiler steam flowrate, kg/s.

Details of each NARX model structure for both output variables using FROLS algorithms are shown in Appendix A. The NARX model was compared with a linear model and nonlinear model developed via the system identification toolbox in Matlab®, against the validation data from the first principle model, based on MPO as shown in Fig 4, which was assessed based on prediction efficiency [25] (see Table 1). This is to establish the advantage of implementing the FROLS-ERR algorithm. Although the idea approach would have been to compare the identified models against experimental data from a real PCC plant, the approach adopted provides more flexibility with the data sampling rate and it is cost-effective. From the assessment, identified NARX model developed using FROLS algorithm contains model terms that capture the system dynamics and gave a better prediction compare to the other models developed.

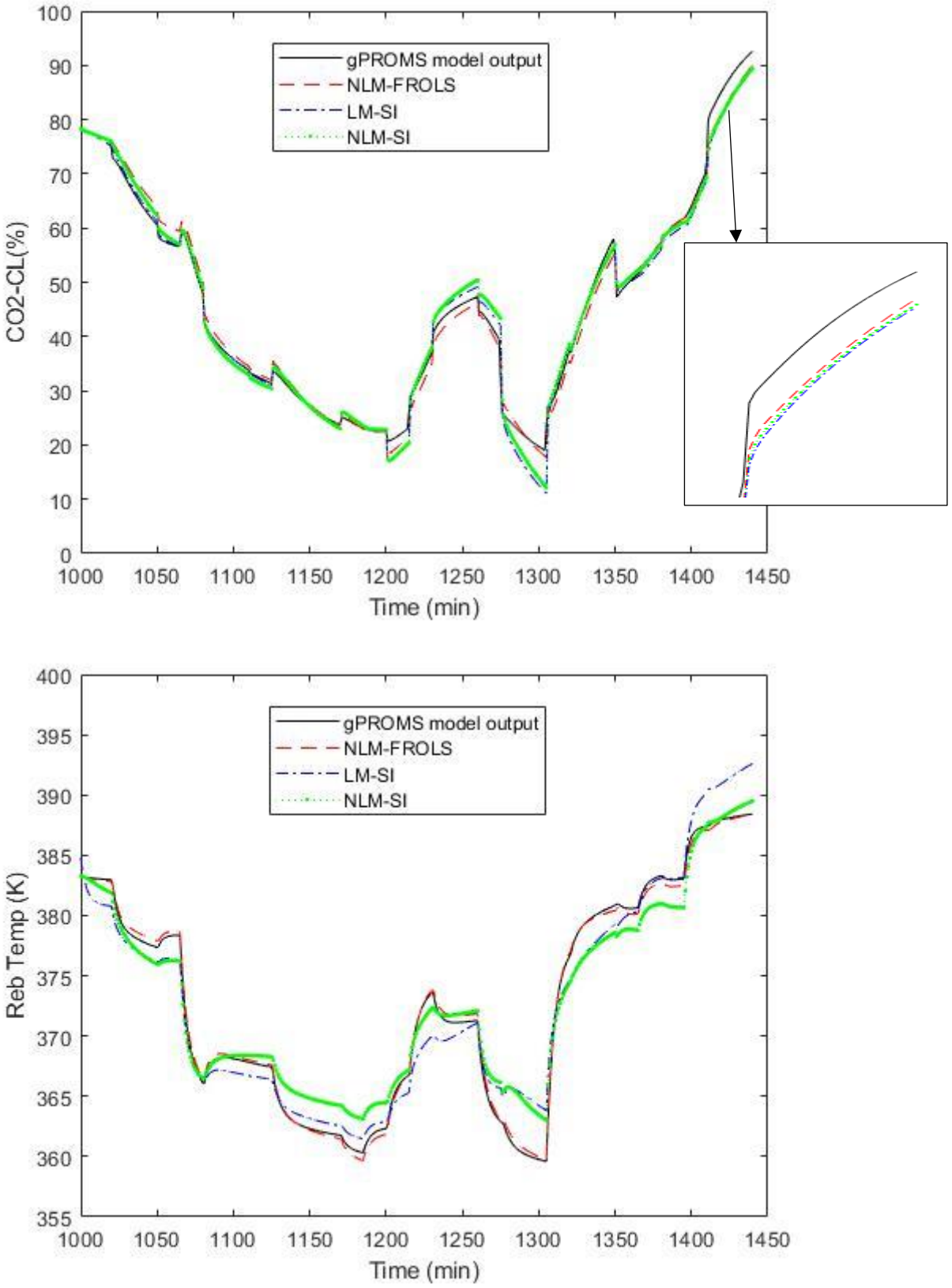

Fig 4 Comparison between MPO data generated by identified models (NLM-FROLS, LM-SI, NLM-SI) and measurements generated by first principle gPROMs model,(a) CO_2 capture level (CO_2-CL); (b) Reboiler temperature (T_{reb}). NLM-FROLS: NARX model developed using FROLS-ERR; LM-SI: ARX model developed using System identification toolbox; NLM-SI NARX model developed using System identification toolbox

Table 1 Prediction efficiency of the Identified NARX model (MPO)

Identified Models	CO_2 capture level (CO_2-CL)	Reboiler temperature (T_{reb})
NLM-FROLS	99.0187	99.8371
LM-SI	96.932	90.4695
NLM-SI	98.7124	95.1024

2.3 Process dynamics analysis

The step response plot for identified NARX model was assessed in comparison with the first principle gPROMS model. This is to ensure that the identified model captures the basic dynamics of the CO_2 capture system. Fig 5 – Fig 7 shows the output response to a 10% step change implemented on each input variable.

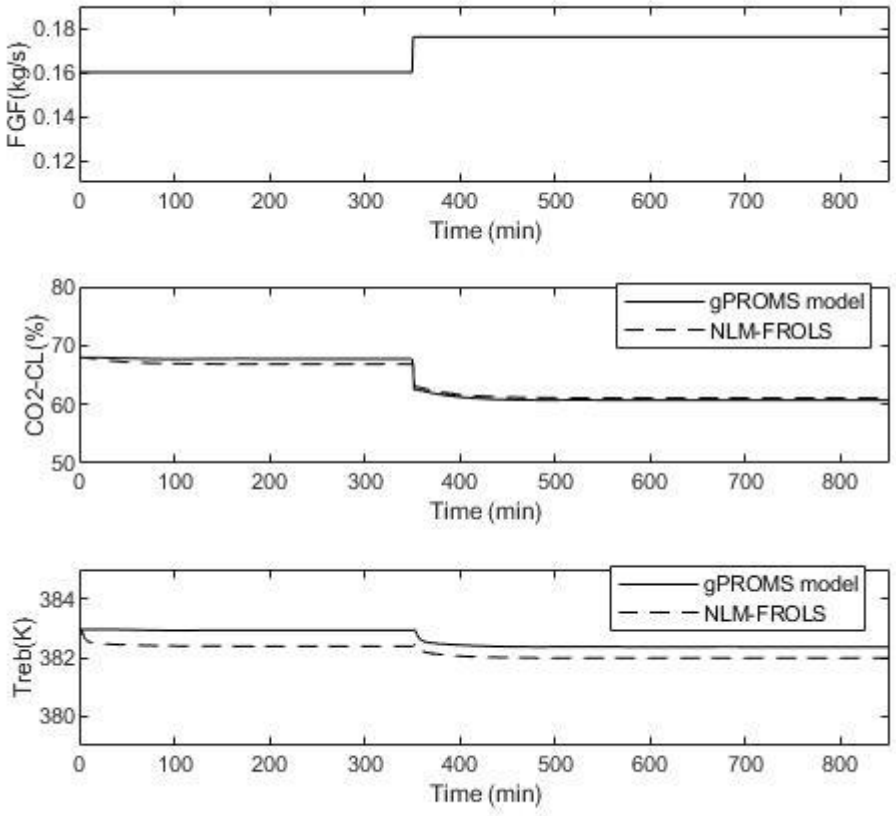

Fig 5 Output response to flue gas flowrate (FGF) (kg/s) increase to the absorber

As highlighted in Fig 5, the flue gas flowrate has an immediate and significant effect on the CO_2 capture level. This is because the CO_2 capture level defined in (1) involves the amount of CO_2 in flue gas. As a result, an increase in flue gas flowrate brings about a drop in CO_2

capture level and vice versa given that the lean solvent flowrate and steam supplied to the reboiler is constant. The effect on the reboiler temperature is minimal and slow.

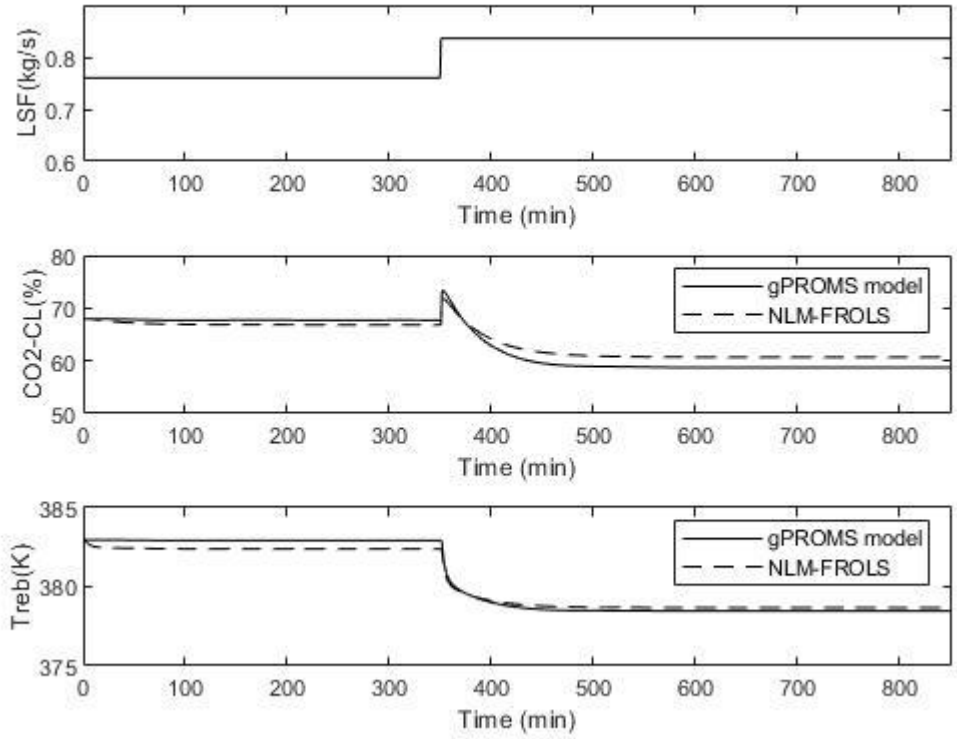

Fig 6 Output responses to a 10% step increase of lean solvent (MEA) flowrate (LSF) (kg/s) to the absorber

Fig 6 revealed that a sharp increase in CO_2 capture level was observed immediately after the step increase was introduced to the lean solvent flowrate. This is accompanied by a slow reduction in the CO_2 capture level until a new steady-state point is attained. This is because, at a constant reboiler steam flowrate, the reboiler temperature is reduced. Thus less CO_2 is stripped of the stripper top[14]. This increases the CO_2 loading in the solvent resulting in a drop in the capture level.

A slow but significant decrease in the reboiler temperature was observed as steam flowrate supplied to the reboiler increases as shown in Fig7. Its influence on the CO_2 capture level and reboiler temperature have large time constants[14]. The dynamic trends of the identified model align with the first principle (gPROMS®) model responses.

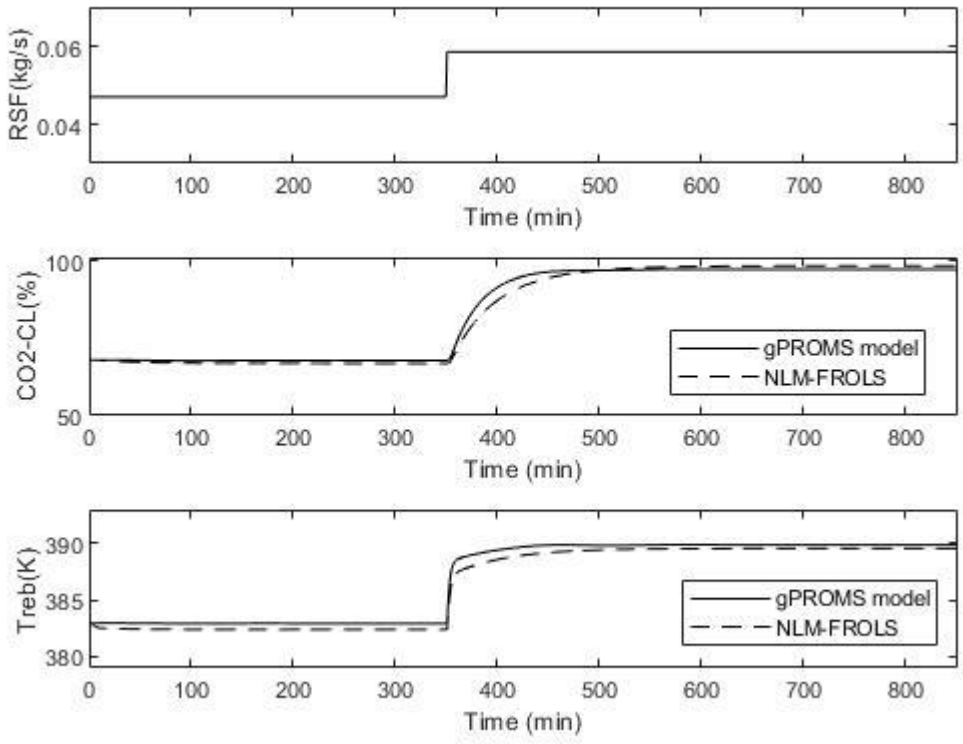

Fig 7 Output responses to a 10% step increase in reboiler steam flowrate (RSF) (kg/s)

3. Multivariable Controller Design

This section discusses the multivariable control design and implementation of the solvent-based PCC process. This study intends to showcase the capability of NMPC strategy to handle the wide variation of CO_2 capture level and disturbances as a result of wide power plant load changes in response to electricity demand in comparison with LMPC control strategy. The schematic diagram of the control design for the solvent-based PCC process is shown in Fig 8 Each control strategy was implemented on the identified model developed in the previous section. Following Sadegh [33] and Kotta & Sadegh [34], the identified model was represented as a classical nonlinear state-space model shown in Eq (4), where $y_1(t)$ and $y_2(t)$ represent CO_2 capture level and reboiler temperature respectively, $u_1(t)$, $u_2(t)$ and $u_3(t)$ represents flue gas flowrate (kg/s), lean solvent flowrate (kg/s) and steam flowrate (kg/s). Details of the nonlinear state-space model in Eq (4) are presented in Appendix B.

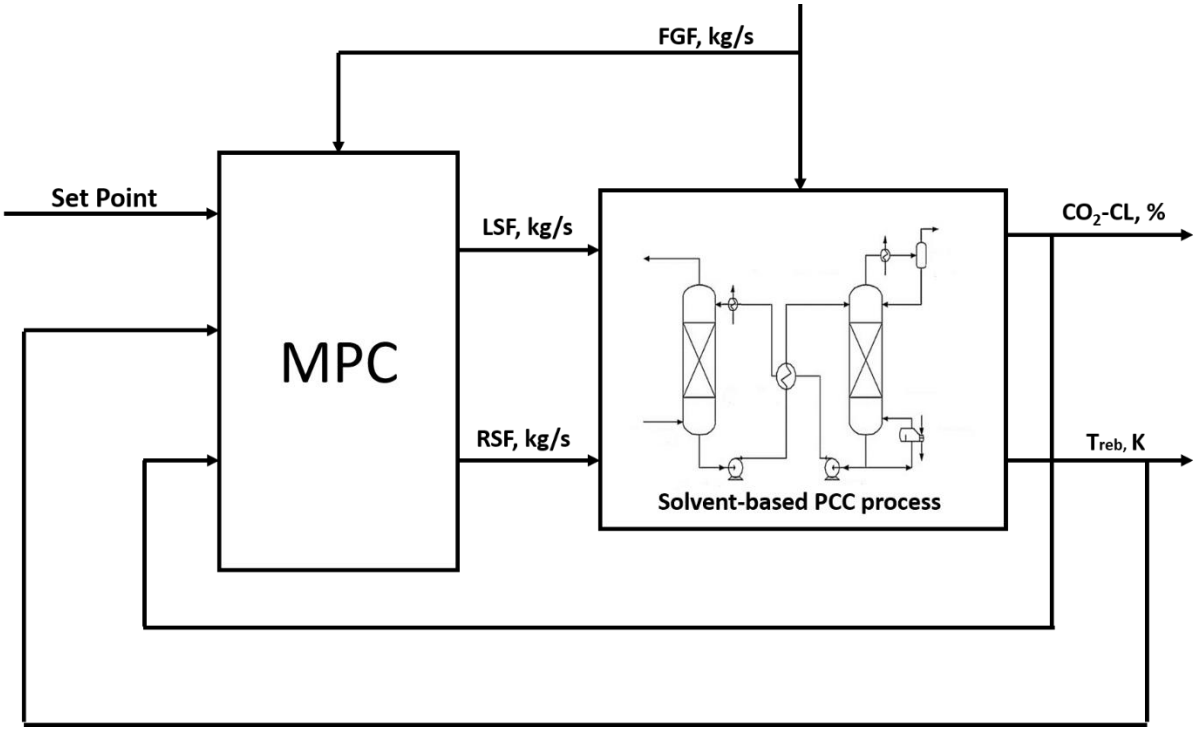

Fig 8 Schematic diagram of MPC control design for the solvent-based PCC process. FGF-fluegas flowrate; LSF: lean solvent flowrate, kg/s; RSF: reboiler steam flowrate, kg/s.

$$x_1(t+1) = x_2(t) + a1x_1(t) + a2x_4(t) + \cdots + a17u_1(t)u_2(t) + a20$$

$$x_2(t+1) = x_3(t) + a3\,x_1(t) + \cdots + a10\,u_1(t) + a18\,u_1(t)u_2(t)$$

$$x_3(t+1) = a8u_2(t) + a11\,u_3(t) + \cdots + a16\,x_1(t+1)u_3(t) + a19x_4(t)u_1(t)$$

$$x_4(t+1) = x_5(t) + b1\,x_4(t) + b3\,u_3(t) + \cdots + b35x_4(t)u_3(t) + b36 \quad (4)$$

$$x_5(t+1) = b2\,x_4(t) + b4\,u_3(t) + b6\,u_3(t)\,u_3(t) + \cdots + b34x_1(t+1)x_1(t)$$

$$y_1(t) = x_1(t)$$

$$y_2(t) = x_4(t)$$

3.1 LMPC formulation

A general formulation for a constrained multivariable LMPC algorithm is expressed below:

$$\min_{\triangle\hat{u},..,\triangle\hat{u}_{t+N_u-1}} \sum_{i=1}^{N_p} (\hat{y}_{t+i} - \hat{r}_{t+i})^T Q(\hat{y}_{t+i} - \hat{r}_{t+i}) + \sum_{i=0}^{N_u} \triangle \hat{u}_{t+i}^T R\Delta\hat{u}_{t+i} \quad (5)$$

Subject to:

$$\hat{x}_{t+1} = A\hat{x}_t + B\hat{u}_t$$

$$\hat{y}_t = C\hat{x}_t$$

$$\hat{y}_{min} \leq \hat{y}_t \leq \hat{y}_{max}$$

$$\hat{u}_{min} \leq \hat{u}_t \leq \hat{u}_{max}$$

$$\triangle \hat{u}_{min} \leq \triangle \hat{u}_t \leq \triangle \hat{u}_{max}$$

where $\hat{y}_{t+i}$ represents the predicted outputs (CO_2 capture level and reboiler temperature) at $(t+i)$th time instant and $\Delta\hat{u}_{(t+1)}^T$ represents manipulated variable rates (lean solvent flowrate and steam flowrate) to achieve the target-controlled variables close to the set-point condition $\hat{r}_{(t+1)}$. The upper and lower bounds for both manipulated and controlled variables are represented as $\hat{y}_{min}, \hat{y}_{max}, \hat{u}_{min}, \hat{u}_{max}$ respectively. The weights assigned to the controlled and manipulated variables rate were represented as Q and R respectively. For LMPC, the nonlinear state-space model was linearized at the nominal operating point shown in Table 2. $\hat{x}_t$ is the state vector of the linear state-space model of the CO_2 capture process at time instant t and *A, B, C* are the model matrices of the linear state space prediction model.

3.2 NMPC formulation

For NMPC, similar optimization objective function as LMPC was adopted as shown in Eq (6). $\hat{x}_t$ represents the current state vector of the nonlinear state-space model of the solvent-based PCC process in Eq (4). Tables 3 and 4 detail the process constraints and formulation parameters for both LMPC and NMPC implemented in Simulink®.

$$\min_{\triangle\hat{u},..,\triangle\hat{u}_{t+N_u-1}} \sum_{i=1}^{N_p} (\hat{y}_{t+i} - \hat{r}_{t+i})^T Q(\hat{y}_{t+i} - \hat{r}_{t+i}) + \sum_{i=0}^{N_u} \triangle \hat{u}_{t+i}^T R\Delta\hat{u}_{t+i}$$

Subject to:

$$\hat{x}_{t+1} = f(\hat{x}_t, \hat{u}_t) \quad (6)$$

$$\hat{y}_{t+1} = g(\hat{x}_{t+1})$$

$$\hat{y}_{min} \leq \hat{y}_t \leq \hat{y}_{max}$$

$$\hat{u}_{min} \leq \hat{u}_t \leq \hat{u}_{max}$$

$$\triangle \hat{u}_{min} \leq \triangle \hat{u}_t \leq \triangle \hat{u}_{max}$$

Table 2 Nominal operating condition

Operating conditions	**Nominal value**
Initial state condition (x_0)	[66.82;41.85; -16.10;382.4;- 9297.8]
Manipulated variables	
Lean solvent flowrate	0.76 kg/s
Steam flowrate	0.047 kg/s
Disturbance variable	
Flue gas flowrate	0.16 kg/s
Output variables	
CO_2 capture level (CO_2-CL)	66.82 (%)
Reboiler Temperature (T_{reb})	382.4K

Table 3 Process constraints

Manipulated variables	$\hat{u}_{min}$	$\Delta\hat{u}_{min}$	$\hat{u}_{max}$	$\Delta\hat{u}_{max}$
Lean solvent flowrate (MV1)	0.1 kg/s	-0.007 kg/s	1.0 kg/s	0.007 kg/s
Steam flowrate (MV2)	0.01 kg/s	-0.001 kg/s	0.1 kg/s	0.001 kg/s
Controlled variables	$\hat{y}_{min}$		$\hat{y}_{max}$	
CO_2 -CL (CV1)	30 (%)		100 (%)	
T_{reb} (CV2)	370 (K)		400 (K)	

Table 4 LMPC and NMPC formulation parameters

N_P		10	
N_u		2	
Weights (Q)		Weights (R)	
MV1	0.1	CV1	1
MV2	0.1	CV2	1

4. Control Performance Evaluation

This section exhibits the control performance of NMPC design for the solvent-based PCC process. The control performance of NMPC was evaluated in comparison with MPC and conventional PID controller under two scenarios, which are:

a) variation in flue gas flowrate
b) Variation in flue gas flowrate and both controlled variable set-points simultaneously.

For each scenario, the control performance was evaluated based on integral squared error (ISE) of the controlled variables against its respective set-points [7] as it is commonly adopted as a performance evaluation measure for solvent-based PCC control[4,7,10]. This is calculated as:

$$ISE(CV) = \int_{t=0}^{t_{final}} (CV_{SP} - CV(t))^2 dt \quad (7)$$

4.1 Case A: variation of flue gas flowrate

This section evaluates the performance of each control strategy on CO_2 capture plant in a scenario where there is fluctuation in the flue gas flowrate, which is a reflection of the power load variation. For this case, it was assumed that at t = 18000s and 36000s, the flue gas flowrate increased/decreased from 0.16kg/s to 0.20kg/s and to 0.12kg/s respectively. This was at ramping rates of 0.42%/min and 0.67%/min respectively. The control objective for this case is to maintain the CO_2 capture level and reboiler temperature at nominal operating condition while the flue gas flowrate is varied.

The closed-loop performance for both LMPC and NMPC is shown in Fig 8. Both LMPC and NMPC were able to reject the flue gas flowrate disturbance which keeping the CVs at nominal conditions. However, NMPC showed an improvement in terms of minimizing the output deviation for both CO_2-CL and T_{reb} by 55.3% and 92.74% respectively in comparison with LMPC. This is reflected in the ISE values shown in Table 5, making NMPC a superior controller compared LMPC in terms of disturbance rejection from flue gas flowrate.

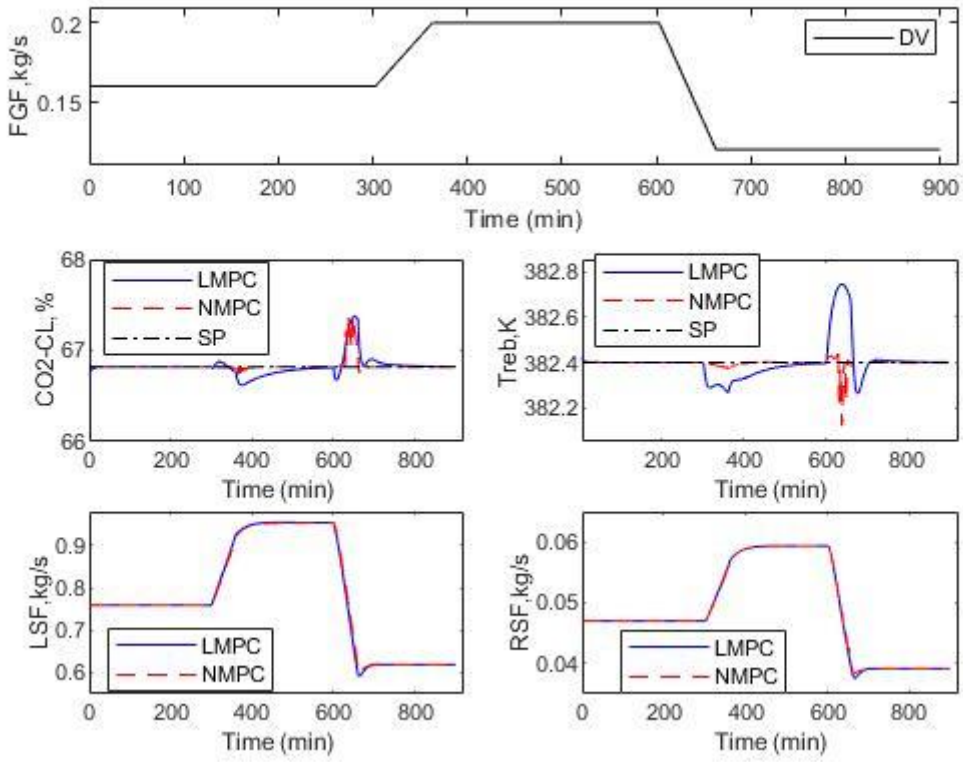

Fig 9 Closed-loop performance to a variation in flue gas flowrate for 15hr (54000s). LMPC – linear model predictive control; NMPC – nonlinear MPC; SP – set point; DV – disturbance variable

Table 5 Summary of the closed-loop control performance evaluation for control schemes (NMPC vs LMPC)

Scenario	ISE			
	NMPC		LMPC	
CVs	CO_2-CL	T_{reb}	CO_2-CL	T_{reb}
Case A	0.0051	5.1514E-04	0.0114	0.0071
Case B	7.5966E+03	680.2141	9.2484E+03	836.4045

4.2 Case B: Variation in both flue gas flowrate and controlled variable set-points simultaneously

The case evaluates the control system performance under a strong variation in the operation of the CO_2 capture process while the power plant operates at a flexible mode. For this case, the CO_2 capture level (CO_2-CL) set-point was varied in the load following manner in response to grid demand along with the same variation of flue gas flowrate in case A.

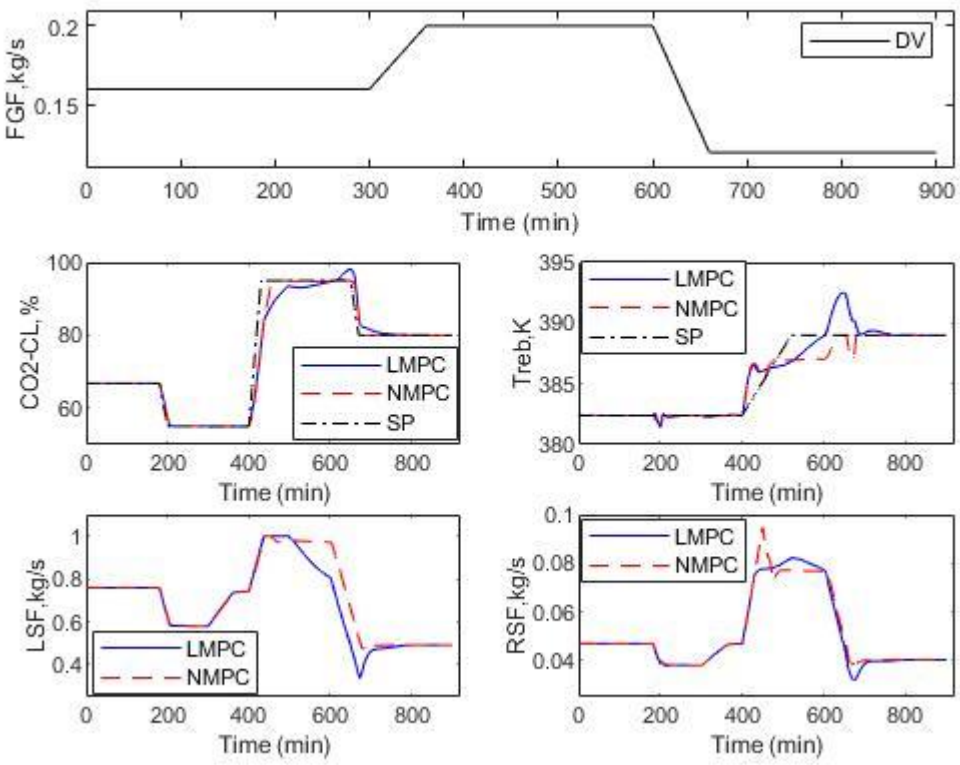

Fig 10 Closed-loop performance to a variation in controlled variable set-points 15hr (54000s). LMPC – linear model predictive control; NMPC – nonlinear MPC

In this case, the CO_2 capture level set point was varied at time t = 10800s from 66.82% to 55%, t = 24000s from 55% to 95%, t = 39000s from 95% to 80% at ramping rates of 0.94%/min,

2.4%/min and 0.79% respectively. In addition, the reboiler temperature set point was increased from 382.2K to 389K at time t= 24000s at a ramping rate of 0.092%/min.

The closed-loop performance of each control strategy is shown in Fig 9. For both controlled variables, NMPC gave better performance compared with LMPC. NMPC was also able to track the set-point quickly in response to the changes in the controlled variables. LMPC was not able to adequately track the controlled variable set-points in quick response time compared to NMPC. The performance evaluation measure ISE shown in Table 7 revealed that NMPC was able to track a wide variation in the controlled variables (CO_2-CL and T_{reb}) by 17.8% and 18.6% respectively compared with LMPC.

5. Conclusion and recommendation for future study

Solvent-based PCC process imposes a limitation on the fossil-fuel power plant's load-following capability when they are integrated due to its large inertia. This challenge could be addressed using a robust control system, which will allow flexible operation of the PCC process in response to power plant load changes without sacrificing the statutory CO_2 capture requirement. In this study, NMPC was developed for this purpose. This was achieved by optimizing the quadratic objective function derived from the prediction model for the PCC process, which was developed as a 3X2 MIMO NARX model using FROLS-ERR algorithm. The developed NMPC was implemented in the PCC process and was evaluated under two cases in comparison with LMPC. The simulation results for Case A showed that NMPC gave a better performance in terms of disturbance rejection by 55.3% and 92.74% for CO_2-CL and T_{reb} respectively. The superior performance of NMPC was also observed in Case B with an improvement of 17.86% and 18.67% for CO_2-CL and T_{reb}. From the simulation results, it was concluded that NMPC is better because the NMPC utilizes the nonlinear model developed using FROLS-ERR algorithm, which can adequately predict the PCC process dynamics at a wide range of flexible operation. Further work will be carried out on uncertainty quantification of the NARX model for NMPC implementation and an assessment of the NMPC performance under a wider range of operation and quicker ramp rate.

Credit authorship contribution statement

Toluleke E Akinola: Conceptualization, Methodology, software, validation, Writing-Original daft preparation. **Eni Oko**: Conceptualization, Supervision, Writing- Reviewing and Editing. **Xiao Wu:** Conceptualization, Writing- Reviewing and Editing. **Keming Ma:** Writing- Reviewing and Editing. **Meihong Wang:** Conceptualization, Supervision, Funding acquisition, Writing-Reviewing and Editing.

Declaration of competing interest

The authors declare that they have no known competing financial interests or personal relationships that could have appeared to influence the work reported in this paper.

Acknowledgement

The UK authors would like to acknowledge financial support from UK EPSRC under the grant of UK *Carbon Capture and Storage Research Centre 2017* (Ref: EP/P026214/1)

Appendix A : Identified Model structure using FROLS algorithm

Table A.1 Identified model structure using FROLS algorithm for CO_2 capture level (CO_2-CL)

s/n	Model Terms	Parameter Estimates	ERR (%)	BIC
1	$y_1(t-1)$	-1.36E-01	9.97E+01	2.86E-03
2	$y_2(t-1)$	8.78E-02	6.12E-02	2.25E-03
3	$y_1(t-2)$	7.66E-01	2.03E-02	2.06E-03
4	$y_2(t-1)*u_1(t-1)$	-8.11E+00	9.06E-03	1.98E-03
5	$y_2(t-1)*u_1(t-2)$	7.58E+00	4.21E-02	1.55E-03
6	$u_2(t-1)$	2.40E+01	2.69E-03	1.53E-03
7	$u_2(t-2)$	-7.77E+00	5.55E-02	9.57E-04
8	$u_2(t-3)$	-1.58E+01	5.40E-03	9.06E-04
9	$u_1(t-1)$	2.84E+03	2.77E-03	8.82E-04
10	$u_1(t-2)$	-2.70E+03	5.44E-02	3.01E-04
11	$u_3(t-3)$	-6.85E+02	1.53E-03	2.87E-04
12	$u_2(t-1)*u_3(t-3)$	6.41E+02	3.38E-04	2.85E-04
13	$u_2(t-2)*u_3(t-3)$	-5.33E+02	3.03E-03	2.54E-04
14	$y_1(t-1)*y_2(t-3)$	9.15E-04	3.15E-04	2.52E-04
15	$y_1(t-3)*y_1(t-3)$	1.76E-03	6.26E-04	2.46E-04
16	$y_1(t-1)*y_1(t-1)$	2.38E-03	3.52E-04	2.44E-04
17	$y_1(t-2)*y_1(t-3)$	-7.82E-03	3.75E-04	2.41E-04
18	constant	-2.99E+01	4.38E-04	2.38E-04
19	$y_2(t-1)*u_3(t-3)$	1.76E+00	3.37E-04	2.36E-04
20	$u_1(t-3)$	7.45E+01	3.18E-04	2.33E-04
21	$y_1(t-2)*u_3(t-3)$	-7.54E-01	3.21E-04	2.31E-04
22	$u_1(t-2)*u_2(t-1)$	-1.22E+03	1.35E-04	2.31E-04
23	$u_1(t-1)*u_2(t-1)$	1.26E+03	1.08E-03	2.20E-04
24	$u_1(t-1)*u_2(t-2)$	-1.23E+03	2.62E-04	2.18E-04
25	$u_1(t-2)*u_2(t-2)$	1.17E+03	2.15E-03	1.94E-04
26	$y_1(t-1)*y_1(t-3)$	3.76E-03	1.54E-04	1.93E-04
27	$y_2(t-3)*u_1(t-3)$	-8.48E-02	1.20E-04	1.93E-04
28	$u_1(t-1)*u_1(t-3)$	6.70E+01	6.09E-05	1.94E-04

Table A.2 Identified model structure using FROLS algorithm for Reboiler temperature (T_{reb})

s/n	Model Terms	Parameter Estimates	ERR (%)	BIC
1	$y_2(t-1)$	-7.48E+00	9.96E+01	3.68E-03
2	$y_2(t-2)$	6.65E+00	2.40E-01	1.35E-03
3	$u_3(t-1)$	-5.53E+02	2.65E-02	1.09E-03
4	$u_3(t-2)$	1.77E+03	8.42E-02	2.61E-04
5	$u_2(t-1)$	7.08E+00	9.02E-04	2.54E-04
6	$u_3(t-1)*u_3(t-2)$	-3.50E+03	8.89E-04	2.47E-04
7	$u_3(t-2)*u_3(t-2)$	2.55E+03	1.00E-02	1.47E-04
8	$y_1(t-2)$	1.25E-01	7.87E-04	1.39E-04
9	$y_1(t-1)$	1.23E-01	2.51E-03	1.15E-04
10	constant	3.32E+02	9.88E-04	1.05E-04
11	$u_2(t-2)*u_3(t-1)$	3.89E+02	1.09E-03	9.44E-05
12	$y_1(t-2)*u_3(t-1)$	3.99E+00	2.48E-03	6.89E-05
13	$u_2(t-2)*u_3(t-2)$	-8.24E+01	1.06E-03	5.82E-05
14	$u_2(t-2)$	3.52E+01	4.94E-04	5.33E-05
15	$y_1(t-2)*u_2(t-1)$	5.04E-02	7.55E-04	4.56E-05
16	$u_3(t-1)*u_3(t-1)$	-1.07E+03	3.86E-04	4.17E-05
17	$y_2(t-2)*u_3(t-2)$	-3.71E+01	2.75E-04	3.90E-05
18	$y_2(t-1)*u_3(t-2)$	3.24E+01	1.14E-03	2.68E-05
19	$u_1(t-2)*u_2(t-1)$	3.38E+00	2.13E-04	2.46E-05
20	$u_2(t-1)*u_2(t-2)$	-1.52E+01	1.11E-04	2.35E-05
21	$y_2(t-1)*u_2(t-2)$	-5.05E-01	2.54E-04	2.09E-05
22	$y_2(t-2)*u_2(t-2)$	3.92E-01	1.02E-04	1.98E-05
23	$y_2(t-2)*y_2(t-2)$	3.31E-02	7.13E-05	1.92E-05
24	$u_1(t-2)*u_1(t-2)$	5.59E+01	7.30E-05	1.85E-05
25	$u_1(t-1)*u_3(t-2)$	1.65E+01	1.16E-04	1.72E-05
26	$y_1(t-2)*u_1(t-2)$	1.54E-01	9.40E-05	1.63E-05
27	$y_1(t-1)*u_3(t-1)$	-5.42E+00	7.82E-05	1.55E-05
28	$y_2(t-1)*y_2(t-1)$	5.40E-02	4.40E-05	1.51E-05
29	$y_2(t-1)*y_2(t-2)$	-8.46E-02	3.49E-05	1.47E-05
30	$y_1(t-2)*y_2(t-2)$	-5.56E-04	2.41E-05	1.45E-05
31	$y_1(t-1)*y_1(t-1)$	-2.76E-04	1.80E-04	1.25E-05
32	$y_1(t-2)*y_1(t-2)$	-7.98E-04	1.15E-04	1.12E-05
33	$y_1(t-1)*u_3(t-2)$	4.38E+00	1.80E-05	1.11E-05
34	$y_2(t-2)*u_3(t-1)$	3.95E+01	4.15E-05	1.06E-05
35	$y_2(t-2)*u_1(t-2)$	-1.35E+00	1.87E-05	1.05E-05
36	$y_1(t-2)*u_3(t-2)$	-3.55E+00	1.56E-05	1.03E-05
37	$u_1(t-1)$	2.30E+00	1.10E-05	1.03E-05
38	$y_1(t-1)*y_2(t-2)$	-1.68E-04	1.28E-05	1.02E-05
39	$y_2(t-1)*u_1(t-2)$	1.31E+00	1.04E-05	1.01E-05
40	$u_1(t-2)*u_3(t-2)$	-2.77E+02	1.46E-05	9.97E-06
41	$u_2(t-1)*u_3(t-1)$	-2.87E+01	1.12E-05	9.88E-06

s/n	Model Terms	Parameter Estimates	ERR (%)	BIC
42	$y_1(t-1)*u_1(t-1)$	-3.58E-01	1.02E-05	9.81E-06
43	$y_1(t-1)*y_1(t-2)$	1.21E-03	5.02E-06	9.81E-06
44	$y_1(t-2)*u_1(t-1)$	3.15E-01	1.71E-05	9.64E-06
45	$y_2(t-1)*u_3(t-1)$	-3.75E+01	4.02E-06	9.65E-06

Appendix B : Nonlinear state-space model represented in Eq (4)

$$x_1(t+1) = x_2(t) + a1x_1(t) + a2x_4(t) + a4x_4(t)u_1(t) + a6u_2(t) + a9u_1(t) + a13x_1(t)x_1(t) + a17u_1(t)u_2(t) + a20$$

$$x_2(t+1) = x_3(t) + a3\,x_1(t) + a5\,x_4(t+1)u_1(t) + a7\,u_2(t) + a10\,u_1(t) + a18\,u_1(t)u_2(t)$$

$$x_3(t+1) = a8u_2(t) + a11\,u_3(t) + a12\,x_1(t)x_1(t) + a14\,x_1(t+1)x_1(t) + a15\,u_1(t) + a16\,x_1(t+1)u_3(t) + a19x_4(t)u_1(t)$$

$$x_4(t+1) = x_5(t) + b1\,x_4(t) + b3\,u_3(t) + b5\,u_2(t) + b8\,x_1(t) + b11u_3(t)u_3(t) + b19x_1(t)u_3(t) + b20x_4(t)x_4(t) + b23x_1(t)x_1(t) + b28\,u_1(t) + b32u_2(t)u_3(t) + b33x_1(t)u_1(t) + b35x_4(t)u_3(t) + b36$$

$$x_5(t+1) = b2\,x_4(t) + b4\,u_3(t) + b6\,u_3(t)\,u_3(t) + b7\,x_1(t) + b9u_2(t)u_3(t) + b10\,u_2(t) + b12x_4(t)u_3(t) + b13x_4(t+1)\,u_3(t) + b14x_4(t+1)\,u_2(t) + b15x_4(t)\,u_2(t) + b16x_4(t)x_4(t) + b17\,u_1(t)\,u_1(t) + b18x_1(t)\,u_1(t) + b21x_4(t+1)x_4(t) + b22x_1(t)x_4(t) + b24x_1(t)x_1(t) + b25x_1(t+1)\,u_3(t) + b26x_4(t)\,u_1(t) + b27x_1(t)\,u_3(t) + b29x_1(t+1)x_4(t) + b30x_4(t+1)\,u_1(t) + b31\,u_1(t)\,u_3(t) + b34x_1(t+1)x_1(t)$$

$$y_1(t) = x_1(t)$$

$$y_2(t) = x_4(t)$$

CO_2 –CL $(x_1(t+1), x_2(t+1), x_3(t+1))$:

a1 = 0.401038365; a2= 0.120907502; a3 = 0.536059372; a4= -3.607965387; a5= 3.153647677; a6= 18.36331491; a7= -6.65601744; a8= -8.423016956; a9= 978.3521546; a10= -835.4354897; a11= 32.17773739; a12= 0.00304912; a13= 0.0037891; a14= -0.006629235; a15= -50.20476452; a16= -0.024865731; a17= 249.5072023; a18= -263.887705; a19= 0.210554405; a20= -45.0649.

T_{reb} $(x_4(t+1), x_5(t+1))$:

b1= -12.3280395; b2= 10.28165535; b3= 2247.864567; b4= -386.1475283; b5= -5.604615654; b6= -302.3773266; b7= -0.563541525; b8= 1.034525008; b9= -19.12868452; b10= -86.90804244;

b11= -1092.942945; b12= 10.67286708; b13= -9.467930137; b14= 0.732315965; b15= -0.514175774; b16= 0.063027613; b17= 40.93231842; b18= 0.20211674; b19= -0.036329361; b20 = 0.093905112; b21= -0.152994737; b22= 0.001759541; b23 = 0.00039346; b24 = -0.001039967; b25 = 0.487551676; b26= -1.92244848; b27= -0.80252386; b28= 5.557376538; b29 = -0.003044387; b30 = 1.880415179; b31= -213.219774; b32= 81.03985604; b33= -0.069305502; b34= 0.000883007; b35= -5.43867; b36 = 587.6837107.

References

[1] Lawal A, Wang M, Stephenson P, Koumpouras G, Yeung H. Dynamic modelling and analysis of post-combustion CO_2 chemical absorption process for coal-fired power plants. Fuel 2010;89:2791–801.

[2] Lindsey R. Climate Change: Atmospheric Carbon Dioxide. NOAA Clim 2019. Available from https://www.climate.gov/news-features/understanding-climate/climate-change-atmospheric-carbon-dioxide (accessed September 23, 2019).

[3] GCCS I. The Global Status of CCS. Glob CCS Inst 2017. Available from https://www.globalccsinstitute.com/wp-content/uploads/2018/12/2017-Global-Status-Report.pdf (accessed September 23, 2019).

[4] Zhang Q, Turton R, Bhattacharyya D. Nonlinear model predictive control and H-∞ robust control for a post-combustion CO_2 capture process. Int J Greenh Gas Control 2018;70:105–16.

[5] Lin YJ, Pan TH, Wong DSH, Jang SS, Chi YW, Yeh CH. Plantwide control of CO_2 capture by absorption and stripping using monoethanolamine solution. Ind Eng Chem Res 2011;50:1338–45.

[6] Lin YJ, Wong DSH, Jang SS, Ou JJ. Control strategies for flexible operation of power plant with CO_2 capture plant. AIChE J 2012;58:2697–704.

[7] Nittaya T, Douglas PL, Croiset E, Ricardez-Sandoval LA. Dynamic modelling and control of MEA absorption processes for CO_2 capture from power plants. Fuel 2014;116:672–91.

[8] Panahi M, Skogestad S. Economically efficient operation of CO_2 capturing process part I: Self-optimizing procedure for selecting the best controlled variables. Chem Eng Process Process Intensif 2011;50:247–53.

[9] Panahi M, Skogestad S. Economically efficient operation of CO_2 capturing process. Part II. Design of control layer. Chem Eng Process Process Intensif 2012;52:112–24.

[10] Hossein Sahraei M, Ricardez-Sandoval LA. Controllability and optimal scheduling of a CO_2 capture plant using model predictive control. Int J Greenh Gas Control 2014;30:58–71.

[11] Gaspar J, Gladis A, Jørgensen JB, Thomsen K, Von Solms N, Fosbøl PL. Dynamic operation and simulation of post-combustion CO_2 capture. Energy Procedia, vol. 86, 2016, p. 205–14.

[12] Wu X, Wang M, Liao P, Shen J, Li Y. Solvent-based post-combustion CO_2 capture for power plants: A critical review and perspective on dynamic modelling, system identification, process control and flexible operation. Appl Energy 2020;257.

[13] Camacho EF, Alba CB. Model predictive control. Springer Science & Business Media; 2013.

[14] Wu X, Shen J, Li Y, Wang M, Lawal A. Flexible operation of post-combustion solvent-based carbon capture for coal-fired power plants using multi-model predictive control: A simulation study. Fuel 2018;220:931–41.

[15] Findeisen R, Allgöwer F. An introduction to nonlinear model predictive control. 21st Benelux Meet. Syst. Control, vol. 11, Technische Universiteit Eindhoven Veldhoven Eindhoven, The Netherlands; 2002, p. 119–41.

[16] Mehleri ED, Dowell NM, Thornhill NF. Model Predictive Control of Post-Combustion CO_2 Capture Process integrated with a power plant. Comput Aided Chem Eng 2015;37:161–6.

[17] Luu MT, Abdul Manaf N, Abbas A. Dynamic modelling and control strategies for flexible operation of amine-based post-combustion CO_2 capture systems. Int J Greenh Gas Control 2015;39:377–89.

[18] He Z, Sahraei MH, Ricardez-Sandoval LA. Flexible operation and simultaneous scheduling and control of a CO_2 capture plant using model predictive control. Int J Greenh Gas Control 2016;48:300–11.

[19] Wu X, Shen J, Li Y, Wang M, Lawal A, Lee KY. Dynamic behavior investigations and disturbance rejection predictive control of solvent-based post-combustion CO_2 capture process. Fuel 2019;242:624–37.

[20] Wu X, Wang M, Shen J, Li Y, Lawal A, Lee KY. Reinforced coordinated control of coal-fired power plant retrofitted with solvent based CO_2 capture using model predictive controls. Appl Energy 2019;238:495–515.

[21] Åkesson J, Laird CD, Lavedan G, Prölß K, Tummescheit H, Velut S, et al. Nonlinear Model Predictive Control of a CO_2 Post-Combustion Absorption Unit. Chem Eng Technol 2012;35:445–54.

[22] Hauger SO, Flø NE, Kvamsdal H, Gjertsen F, Mejdell T, Hillestad M. Demonstration of non-linear model predictive control of post-combustion CO_2 capture processes. Comput Chem Eng 2019;123:184–95.

[23] Patron GD, Ricardez-Sandoval L. A robust nonlinear model predictive controller for a post-combustion CO_2 capture absorber unit. Fuel 2020;265.

[24] Wu X, Shen J, Wang M, Lee KY. Intelligent predictive control of large-scale solvent-based CO_2 capture plant using artificial neural network and particle swarm optimization. Energy 2020;196:117070.

[25] Akinola TE, Oko E, Gu Y, Wei H-L, Wang M. Non-linear system identification of solvent-based post-combustion CO_2 capture process. Fuel 2019;239:1213–23.

[26] Biliyok C, Lawal A, Wang M, Seibert F. Dynamic Validation of Model for Post-Combustion Chemical Absorption CO_2 Capture Plant. Comput Aided Chem Eng 2012;30:807–11.

[27] Davis J, Rochelle G. Thermal degradation of monoethanolamine at stripper conditions. Energy Procedia 2009;1:327–33.

[28] Lawal A, Wang M, Stephenson P, Obi O. Demonstrating full-scale post-combustion CO_2 capture for coal-fired power plants through dynamic modelling and simulation. Fuel 2012;101:115–28.

[29] Li P, Wei H-L, Billings SA, Balikhin MA, Boynton R. Nonlinear model identification from multiple data sets using an orthogonal forward search algorithm. J Comput Nonlinear Dyn 2013;8:41001.

[30] Billings SA. Nonlinear system identification: NARMAX methods in the time, frequency, and spatio-temporal domains. University of Sheffield, United Kingdom: wiley; 2013.

[31] Wei HL, Billings SA, Liu J. Term and variable selection for non-linear system identification. Int J Control 2004;77:86–110.

[32] Wei HL, Billings SA. Improved model identification for non-linear systems using a

random subsampling and multifold modelling (RSMM) approach. Int J Control 2009;82:27–42.

[33] Sadegh N. Minimal realization of nonlinear systems described by input-output difference equations. IEEE Trans Automat Contr 2001;46:698–710.

[34] Kotta Ü, Sadegh N. Two approaches for state space realization of narma models: bridging the gap. Math Comput Model Dyn Syst 2002;8:21–32.